Monitoring T-Lymphocyte Trafficking in Tumors Undergoing Immune Rejection

De-En Hu, Mikko I. Kettunen, and Kevin M. Brindle*

Activated T cells, isolated from animals that had rejected a tumor (E.G7-OVA) expressing chicken ovalbumin, were labeled with citrated superparamagnetic iron oxide nanoparticles at an intracellular iron concentration of up to 0.5 pg/cell. Injection of these labeled T cells into animals bearing E.G7-OVA tumors undergoing immune rejection resulted in tumor infiltration of these cells, which was detectable as a heterogeneous decrease in intensity in T_2-weighted MR images. T-cell infiltration was confirmed by immunohistochemical staining of tumor sections obtained postmortem and was shown to colocalize with iron that had been stained using Prussian blue. Tumor rejection was correlated with the uptake of labeled T cells, since the infiltration of labeled T cells was only observed in those tumors that went on to regress. This technique should assist in the elucidation of those factors that are important in mediating tumor immune rejection. Magn Reson Med 54:1473–1479, 2005.

Key words: cell imaging; magnetic resonance; lymphoma; oval bumin; iron oxide

Studies of tumor immunotherapy have so far failed to demonstrate a consistent correlation among the number, persistence, localization, and antigen responsiveness of vaccine-elicited or adoptively transferred T cells and tumor response. More dynamic methods for monitoring T cell infiltration of tumors, it has been suggested, may help to explain this lack of correlation and furthermore could be used to develop methods that improve T-cell homing to tumors (1).

The immunogenic tumor model, E.G7-OVA, which expresses on its surface an eight-residue peptide of chicken ovalbumin in association with the MHC class I molecule H-2K^b (2,3), has been widely used in studies of immune responses to tumors (4–8). Adoptive transfer experiments with CD8+ T cells that recognize the ovalbumin peptide have demonstrated that these cells can in inhibit tumor growth (4) and, under circumstances where there was tumor rejection, this was accompanied by an increase in the number of CD8+ T cells in the tumor (5). Furthermore, control of E.G7-OVA tumor growth was shown to depend on retention of CD8$^+$ T cells, as tumor growth continued when the cells migrated out of the tumor into the spleen and draining lymph nodes (6). We have shown previously that the immunogenicity of this tumor can be titrated by selecting cells that express different levels of surface ovalbumin. Tumors expressing higher levels of ovalbumin show slower growth and, at sufficiently high levels, undergo immune-mediated regression from about 10 days after tumor implantation. Using this model we have shown that tumor regression is accompanied by a vascular proliferation that can be detected using dynamic contrast agent enhanced MRI and suggested that this technique could be used clinically to provide an early indication of a positive response of tumors to immunotherapy (9). We further showed that there was increased CD8+ T cell infiltration in regressing tumors and that tumor cell death is caused by tumor-cell-derived nitric oxide (NO), the production of which may be stimulated by cytokines secreted by infiltrating immune cells (10). We also showed that uric acid, which is secreted by the dying tumor cells, could have an adjuvant effect, stimulating the immune response to the tumor (11). In view of the importance of T-cell localization in mediating tumor regression, we have sought to develop a MRI method for the noninvasive dynamic tracking of T cells within the tumor microenvironment.

A potential limitation of T-cell tracking by MRI is the relatively inefficient uptake of label by lymphocytes, due to the low efficiency of endocytosis in these cells. However, several methods have been employed to increase uptake. Derivatization of a superparamagnetic iron-oxide-based nanoparticle with a peptide sequence from HIV-1 transactivator protein (Tat) was shown to dramatically enhance T-cell labeling and intracellular iron concentrations as high as 0.7 pg/cell have been reported (12,13). Using dextran-coated superparamagnetic iron oxide nanoparticles (ferumoxides) and an agent that is used as a cationic cell transfection agent (protamine sulfate), Arbab et al. (14) achieved an iron concentration in mouse splenocytes of 1.5 pg/cell. We have used here a relatively simple to prepare citrated anionic iron-oxide-based nanoparticle, similar to that described in Ref. (15), and have achieved intracellular iron concentrations of 1.4 pg/cell in a mouse splenocyte preparation and 0.5 pg/cell in purified T cells. We show here that tumor infiltration of adoptively transferred activated T cells, which have been labeled with these nanoparticles, can be monitored by MRI and that tumor infiltration by these cells is correlated with cell activation and tumor regression.

MATERIALS AND METHODS

Cell Lines and Tumor Implantation

The E.G7-OVA cell line was derived from a murine thymoma line, EL-4, by transfection with a neomycin-selectable vector expressing full-length chicken ovalbumin (2). The E.G7-OVA and EL-4 cells used in this study were taken from frozen stocks held at GlaxoSmithKline, Steve-

Department of Biochemistry, University of Cambridge, Cambridge, United Kingdom.

Grant sponsor: Cancer Research UK; Grant number: C197/A3514.

Correspondence to: K. M. Brindle, Department of Biochemistry, University of Cambridge, 80 Tennis Court Road, Cambridge CB2 1GA, UK. E-mail: kmb@mole.bio.cam.ac.uk

Received 1 March 2005; revised 16 August 2005; accepted 17 August 2005.
DOI 10.1002/mrm.20717
Published online 7 November 2005 in Wiley InterScience (www.interscience.wiley.com).

nage, UK. The cells were cultured as a suspension in RPMI 1640 medium (Invitrogen Ltd., Paisley, UK) containing 10% heat-inactivated fetal calf serum (FCS) (PAA Laboratories, GmbH Linz, Austria), 2 mM L-glutamine, penicillin (100 units/mL), and streptomycin (100 μg/mL).

Wild-type female C57BL/6 mice were purchased at 6–8 weeks of age from Charles River Ltd. (UK). Tumor cells (5×10^6) were injected subcutaneously into the shaved flanks of the animals. Tumor size is reported as the product of the two largest perpendicular diameters (in square millimeters). All experiments were conducted in compliance with a project license issued under the Animals (Scientific Procedures) Act 1986 and were designed with reference to the UKCCCR guidelines for the welfare of animals in experimental neoplasia. The work was approved by a local ethical review committee.

Synthesis of Citrated Magnetic Nanoparticles

Citrated magnetic nanoparticles were prepared as described in Refs. (15–17), with some minor modifications. Briefly, 20 g ferrous chloride ($FeCl_2.4H_2O$) was dissolved in 50 mL 2 M HCl and 32 g ferric chloride ($FeCl_3.6H_2O$) in 200 mL 2 M HCl. The two solutions were mixed and stirred vigorously for 15 min and then 300 mL ammonium hydroxide solution (29%) was added slowly. A black precipitate formed, which was sedimented by placing the vessel containing the suspension over a magnet. The supernatant was decanted, the remaining solution centrifuged for 10 min at 300*g,* and the supernatant discarded. The magnetic particles were then freeze-dried and ground using a mortar and pestle. Twenty grams of the particles was dispersed in 400 mL deionized water and sodium citrate was added (10% per mole of iron) and the solution was stirred for 15 min. The citrated magnetic nanoparticles were then freeze-dried and ground into a fine powder.

Cell Labeling with Magnetic Nanoparticles

Mice were effectively immunized against ovalbumin by implanting them with E.G7-OVA tumor cells expressing relatively high levels of surface ovalbumin. Spleens were collected 30 days after the animals had rejected the E.G7-OVA tumor and washed in complete RPMI 1640 culture medium, which contained glutamine and 10% FCS, and the splenocytes were released by mechanical dissociation. Cells from five spleens were harvested by centrifugation, incubated for 1 min on ice in a red cell lysis buffer (154 mM NH_4Cl, 10 mM $KHCO_3$, 0.15 mM EDTA), and then resuspended in fresh culture medium. Splenocytes collected from animals implanted with E.G7-OVA tumors, expressing lower levels of surface ovalbumin and that had not undergone immune rejection, were used as controls. T lymphocytes were purified from the splenocyte preparations using a Ficoll 400 density gradient (Sigma) (18).

Lymphocytes that had been cultured for 24 h in complete RPMI 1640 medium were suspended in the same medium (10^6 cells/mL) containing 5 mM sodium citrate. They were then incubated at 37°C with the citrated magnetic nanoparticles, at an iron concentration of 10 mM, for up to 24 h. Following incubation the free magnetic nanoparticles were sedimented by placing a magnet under the vessel containing the cell suspension and the supernatant, containing the cells, was removed and the cells were washed three times in complete RPMI medium containing 5 mM citrate. The cells were then harvested before use in vitro or injection into animals via ip injection (10^7 cells in 0.2 mL).

Magnetic Resonance Imaging

Experiments were performed in a 9.4-T vertical bore magnet (Oxford Instruments) interfaced to a Varian Associates INOVA spectrometer using a whole-body probe (Doty Scientific). Data were collected in vitro and in vivo using a T_2-weighted multislice spin-echo imaging sequence. (Repetition time 2 s; echo-time 21 ms (transverse slices) or 30 ms (coronal slices); field of view 30 mm; 256×128 data matrix; slice thickness 2.0 mm; 21 transverse and 7 coronal slices, with no gaps between the slices.) For experiments in vivo, six animals were used in each group, where the groups were animals bearing regressing tumors injected with activated and labeled T cells; animals bearing regressing tumors injected with nonactivated and labeled T cells; animals bearing nonregressing tumors injected with activated and labeled T cells; and animals bearing regressing tumors injected with activated but unlabeled T cells. Animals were anesthetized by ip injection of Hypnorm (Jansen Pharmaceuticals)/Hypnovel (Roche)/dextrose-saline in the ratio 5:4:31 (10 mL kg^{-1} body wt), and the body temperature of the animals was maintained by blowing warm air through the magnet bore.

Determination of Iron Concentration

Cells were washed in phosphate-buffered saline (PBS) and then 2×10^7 cells were resuspended in 1 mL of PBS containing 1% Triton X-100. After a 15-s homogenization using an Omni GLH-220 homogenizer (Omni International, Inc., Warrenton, VA, USA), the resulting extracts were mixed with 0.9 mL of 4 M HCl and 0.1 mL of 2 M H_2O_2 and incubated at room temperature for 30 min. The extracts were then centrifuged for 5 min at 2000*g* and 0.5 mL of the supernatant was added to 0.5 mL 1.5 M KSCN. Iron forms a complex that absorbs at 447 nm when reacted with thiocyanate ion and this was measured either in a spectrophotometer or by using a plate reader. Ferric chloride was used as a standard (19,20).

Histology and Immunohistochemistry

Tumors were fixed in fresh 10% formalin and embedded in paraffin. Five-micrometer-thick sections were cut and stained with hematoxylin and eosin (H&E) (Sigma) and Prussian blue stain, for ferric ion. Sections were stained for CD8+ T cells, using a rabbit polyclonal antibody recognizing CD8-α (Santa Cruz Biotechnology, Inc., Santa Cruz, CA, USA). This primary antibody was detected using a biotinylated anti-rabbit IgG secondary antibody and horseradish peridase (HRP) conjugated to streptavidin (Santa Cruz Biotechnology) or a fluorescein isothiocyanate (FITC)-conjugated monoclonal secondary antibody that recognized rabbit IgG (Sigma, Gillingham, Dorset, UK). As a negative control, the sections were treated with nonim-

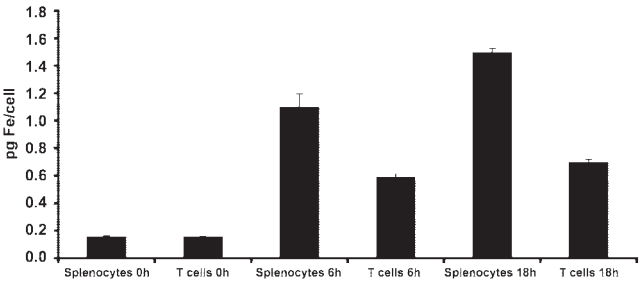

FIG. 1. Quantification of iron uptake by splenocytes and T cells. Cells were incubated at a density of 10^7 cells/mL for the indicated time at 37°C in RPMI medium containing 2 mM glutamine, 10% FCS, 5 mM citrate, and magnetic nanoparticles at an iron concentration of 10 mM. Cell iron content was determined spectrophotometrically in cell extracts and is quoted as the mean ± SEM ($n = 4$).

mune rabbit serum in place of the primary antibodies. For determination of the extent of iron or CD8-α staining, sections were examined at 133× magnification and the images, with a field of view of 1.2 mm^2, were relayed to a computer for subsequent analysis. The extent of iron or CD8-α staining, expressed as a percentage of the area of the observed tumor section, was determined using ImageJ software (NIH).

RESULTS

Quantification of Iron Uptake and Detection by MRI in Vitro

Splenocytes or T cells (at 10^7 cells/mL) were incubated with the citrated magnetic nanoparticles at an iron concentration in the incubation medium of 10 mM for between 0 and 24 h (Fig. 1). Although this is a higher iron concentration than has been used to obtain cell uptake with cell transfection agents (14,21), the agent is relatively easy and inexpensive to prepare and produced no detectable T-cell toxicity following transfer of the cells into tumor-bearing animals. Iron uptake was determined by spectrophometric analysis of the iron content of cell homogenates. The maximum concentration of iron in the splenocyte preparations was 1.4 pg/cell and that in the isolated T cells was 0.5 pg/cell. The iron concentration in the splenocytes is comparable to a concentration determined previously in splenocytes incubated with a similar particle preparation (15). The sensitivity of the labeled T cells to detection by MRI was determined by imaging phantoms containing between 1 and 10^6 cells /mL, immobilized in 10% gelatin (Fig. 2). There was a measurable decrease in total image intensity at a cell density of 10^4 cell/mL, corresponding to a detection threshold in vitro of <3 cells/voxel. This is comparable to what was observed previously for T cells labeled with Tat peptide-derivatized magnetic nanoparticles (13).

Tumor Recruitment of Labeled T Cells Can Be Visualized by MRI

Tumor infiltration of labeled T cells was visible as heterogeneous regions of hypointensity in T_2-weighted images. At between 1 and 4 days after ip injection of 10^7 labeled and activated T cells there were significant reductions in signal intensities in images obtained from EG.7-OVA tumors undergoing regression (Figs. 3a, b, and c; the images are from three different tumors), but not in the nonregressing tumors (Fig. 3d). Trafficking of labeled T cells into a regressing tumor was not observed if the cells had not been activated, that is isolated from animals that had failed to reject their E.G7-OVA tumor (Fig. 3e). There was also no change in tumor image intensities if the injected activated T cells had not been labeled with magnetic nanoparticles (data not shown). The animals were divided into four groups and six animals were used in each group (the groups are described under Materials and Methods). Representative images from three of these four groups are shown in Fig. 3. These experiments demonstrated that the regions of hypointensity in the images are not simply explained by tumor hemorrhage.

Histochemical Detection of Iron and Infiltrating T Cells in Regressing Tumors

Regressing tumors showed regions where there were large numbers of apoptotic cells, which were readily detectable in H&E-stained sections through the presence of condensed and fragmented nuclei (Fig. 4i and ii). Tumor sections from regressing EG.7 OVA tumors were stained with anti-CD8 antibody. There was significantly greater infiltration of CD8+ T cells in regressing tumors (Fig. 4iv) when compared to nonregressing tumors (Fig. 4iii). The area stained with the anti-CD8 antibody corresponded to 8.7 ± 0.5% of the total area in regressing tumors, compared to 0.9 ± 0.3% in the nonregressing tumors (±SEM, $P < 0.01$, six fields-of-view in three sections from each of three tumors in each group). This is in agreement with previous work from this laboratory (9,10). Trafficking of labeled T cells into tumors was confirmed by staining tumor sections for iron with Prussian blue. Iron staining was observed in

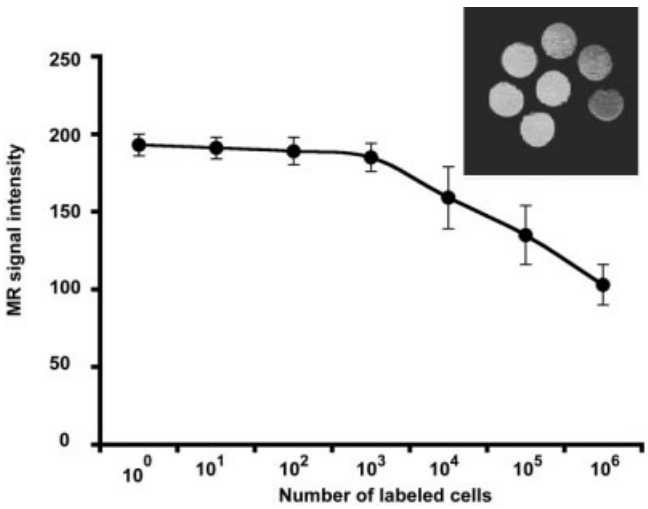

FIG. 2. MRI detection of labeled T cells in vitro. Between 1 and 1 × 10^6 labeled T cells/mL were immobilized in 10% gelatin in 5-mm-diameter NMR tubes and imaged using a T_2-weighted spin echo sequence. The integrated image signal intensity is plotted against the number of labeled cells. The insert shows the MR images from which these intensities were derived.

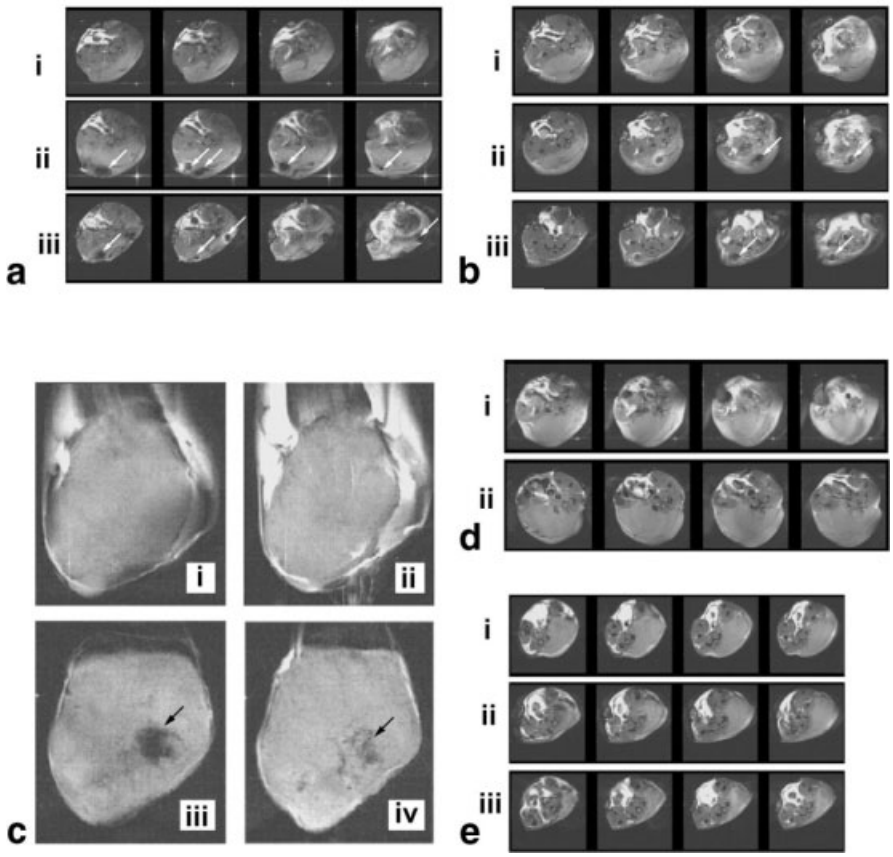

FIG. 3. Tumor trafficking of iron-labeled T cells Successive transverse images (**a** and **b**) and coronal images (c) acquired from three different regressing tumors following injection of T cells purified from splenocyte preparations that had been collected from animals that had rejected an E.G7-OVA tumor and that had been labeled with citrated magnetic nanoparticles. The images in a and b are the corresponding slices (2 mm thick) acquired before ip injection of the labeled cells (i) and at 2 days (ii) and 4 days (iii) after injection. Areas showing loss of signal intensity are arrowed. The images in (c) are the corresponding slices acquired before injection (i) and (ii) and 2 days after injection, (iii) and (iv), respectively. Areas showing loss of signal intensity are arrowed. Successive transverse images (**d**) acquired from a nonregressing tumor following injection of T cells purified from splenocytes that had been collected from animals that had rejected an E.G7-OVA tumor and that had been labeled with citrated magnetic nanoparticles. The images are the corresponding slices (2 mm thick) acquired before injection of the labeled cells (i) and 2 days (ii) after injection of the labeled cells. Successive transverse images (**e**) acquired from a regressing tumor following injection of labeled T cells that had been purified from splenocytes collected from animals that had failed to reject their E.G7-OVA tumor. The images are the corresponding slices (2 mm thick) acquired before injection of the labeled cells (i) and at 2 days (ii) and 4 days (iii) after injection of the labeled cells.

tumor sections of regressing E.G7 OVA tumors that had been taken from animals that had been injected with activated and labeled T cells (Figs. 4v and vi). The area stained represented 7.5 ± 0.3% (SEM) of the total area in 27 fields of view taken from three different tumors. Significant levels of iron were not detectable in sections from tumors that had failed to regress (Fig. 4vii), in regressing tumors from animals that had been injected with unlabeled T cells (data not shown), or in regressing tumors in animals that had been injected with labeled but nonactivated T cells (Fig. 4viii). Staining of consecutive 5-μm sections for T cells, with a rabbit polyclonal antibody recognizing CD8-α and a FITC-conjugated monoclonal secondary antibody that recognized rabbit IgG (Fig. 4ix), and for iron, with Prussian blue (Fig. 4x), showed that iron staining colocalized with regions containing T cells in regressing tumors. Control experiments, in which the sections were first treated with nonimmune rabbit serum and then with the FITC-conjugated monoclonal secondary antibody, showed no detectable fluorescence (data not shown).

DISCUSSION

The introduction of cell-based therapies for treating degenerative, malignant, and genetic diseases has lead to a rapidly growing interest in methods for detecting the migration of cells in vivo using noninvasive MRI methods (22). In the field of cancer therapy, adoptive transfer of tumor antigen-specific lymphocytes has been used in the treatment of several malignancies (23–25). The facility to detect migration of activated T cells into tumors in the clinic should be useful in evaluating the efficacy of these treatments and may also assist in the development of more effective anti-tumor vaccines (1,26).

Methods used to study lymphocyte tracking include labeling cells with fluorescent or bioluminescent (luciferase) probes or with radioisotopes (27–29). The optical methods, which have limited depth penetration, are not well suited to clinical studies and the nuclear imaging methods (positron emission tomography and single-photon emission computed tomography), which are in use clinically, have limited spatial resolution and require the use of radiochemicals that can have significant cellular toxicity and whose short-half-life allows imaging for only 24–48 h. MRI is clinically applicable, allows imaging at relatively high resolution, and can be used to track labeled cells over prolonged periods of time.

A problem with tracking T cells by MRI has been their relatively low uptake of superparamagnetic cell labels and several methods have been used to improve this (12–15). The citrated magnetic nanoparticles used here are relatively simple to prepare and have yielded iron concentrations in purified T cells of up to 0.5 pg/cell. The MRI detection limit for these labeled T cells in vitro, <3 cells/voxel, was comparable with that observed previously for T cells labeled with Tat peptide-derivatized nanoparticles (13). Previous studies on hybridoma cells, labeled with a similar iron oxide preparation, showed no evidence of toxicity from the label and there was reported to be no difference in antibody secretion between labeled and unlabeled cells (15). The iron content of labeled hybridoma cells recovered from the spleens of animals was significantly lower than that of the injected cells, indicating that the labeled cells had retained their proliferative capacity in vivo. We did not test the viability of the labeled T cells used in this study in vitro; however, their facility, when activated, to migrate into the tumor interstitium within 24 h of injection, demonstrated that the labeled cells had retained both viability and function.

Previous work by others has shown that CD8+ T cells can inhibit the growth of E.G7-OVA tumors and even eradicate established tumors (5). Adoptive transfer experiments using CD8+ T cells from OT-1 mice, which have a transgenic T cell receptor specific for H-2K^b and an ovalbumin peptide (257–264), have demonstrated the role of different CD8 effector cells in controlling tumor growth (7). These studies have also demonstrated that control depends on continued retention of CD8+ T cells within the tumor (6). We have shown previously that E.G7-OVA tumors have increased immune cell infiltration, including CD8+ T cells, compared to the untransfected EL4 tumor and that the degree of infiltration is positively correlated with the incidence of immune-mediated regression (9,10). We have shown here that activated T cells, isolated from animals that had rejected an E.G7-OVA tumor, can be labeled with citrated iron oxide nanoparticles and that their migration into an E.G7-OVA tumor, following ip

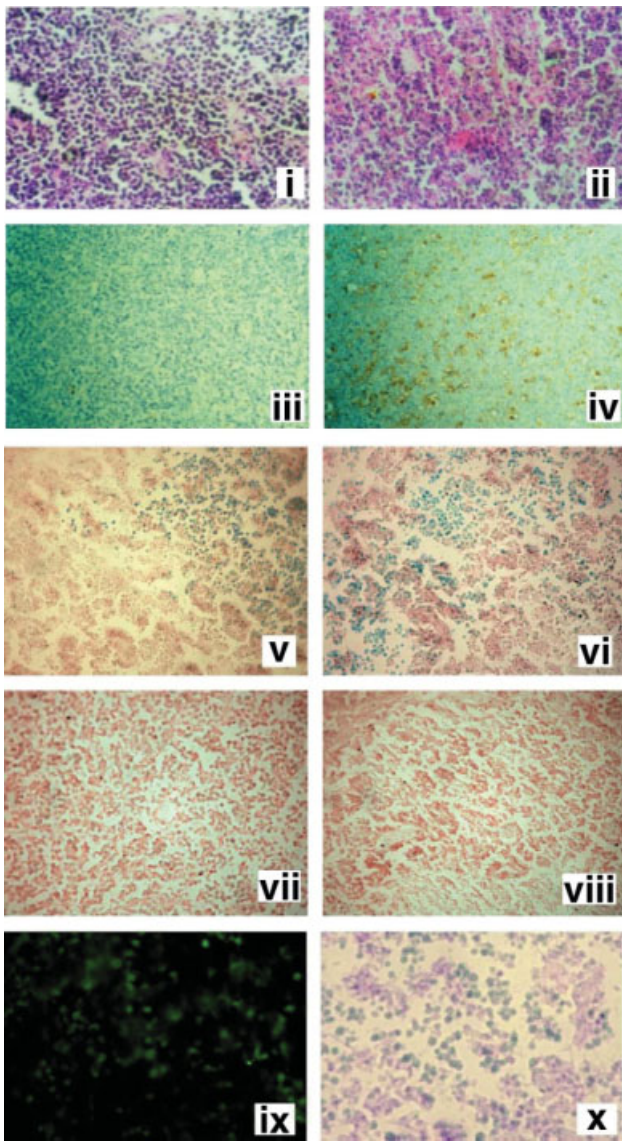

FIG. 4. Histologic assessment of tumor infiltration by T cells and iron labeling. Sections from a nonregressing E.G7-OVA tumor (i) and a regressing E.G7-OVA tumor (ii) stained with hemotoxylin and eosin (H&E) (200× magnification). Sections from a nonregressing E.G7-OVA tumor (iii) and a regressing E.G7-OVA tumor (iv) stained with a rabbit polyclonal anti-CD8 antibody and a biotinylated anti-rabbit IgG secondary antibody and horseradish peroxidase (HRP) conjugated to streptavidin. The sections shown in (iii) and (iv) were counterstained with Light Green (120× magnification). (v) and (vi) show tumor sections from two different tumors, stained for iron with Prussian blue (160× magnification), that had been taken from regressing E.G7-OVA tumors, which had been excised from animals that had received injections of activated and labeled T cells. The sections were counterstained with hematoxylin. (vii) shows a section taken from a nonregressing tumor following injection of T cells purified from splenocytes that had been collected from animals that had rejected an E.G7-OVA tumor and that had been labeled with citrated magnetic nanoparticles. The section was stained with Prussian blue and counterstained with hematoxylin. (160× magnification). (viii) shows a section taken from a regressing tumor following injection of labeled T cells that had been purified from splenocytes collected from animals that had failed to reject their E.G7-OVA tumor. The section was stained with Prussian blue and counterstained with hematoxylin (160× magnification). (ix) shows a fluorescence image and (x) a light field image. Section (ix) was stained with a rabbit polyclonal anti-CD8 antibody and a goat anti-rabbit IgG secondary antibody conjugated with FITC. Section (x) was stained with Prussian blue and counterstained with hematoxylin (320× magnification).

injection of the cells, can be monitored in vivo using MRI (Fig. 3). Tumor infiltration of labeled T cells was only observed in those E.G7-OVA tumors that subsequently underwent regression and was not observed with T cells isolated from animals that had failed to reject their E.G7-OVA tumor (Fig. 3e). Staining of tumor sections obtained postmortem with anti-CD8 antibody showed that there was significantly greater (~10×) infiltration of CD8+ T cells in regressing tumors compared to nonregressing tumors, consistent with previous work from this laboratory and that of others (5,9,10). Staining of tumor sections for iron showed that iron content was increased in regressing tumors in animals that had been injected with activated and iron-labeled T cells and that the iron and T cells were colocalized. Thus, we conclude that the hypointense regions in the MR images are due to the presence of iron-labeled and activated T cells.

There was a previous study in which MRI was used to monitor the trafficking of CD8+ T cells into an immunogenic tumor model, in which the model tumor antigen was also chicken ovalbumin (13). However, there are some important differences between this previous study and that reported here. In this previous study the cells were labeled using a Tat peptide-derivatized nanoparticle, whereas we used a citrated nanoparticle preparation that is relatively simple and inexpensive to prepare and that gives levels of cell labeling that are comparable to those observed in the earlier study. Kircher et al. (13) used T cells that had been harvested from OT-1 mice. These mice, which possess T cells that express a transgenic T-cell receptor that recognizes the SINFEKL peptide from ovalbumin, give T-cell preparations containing over 90% ovalbumin-specific cells (8). These cells were activated in vitro by treatment with SINFEKL peptide and antigen-presenting cells that had been treated with IL-2. We used a heterogeneous T-cell preparation from wild-type mice in which the CD8+ T cells recognizing ovalbumin had been activated in vivo by inoculating the animals with a tumor expressing relatively high levels of ovalbumin and which these animals had subsequently immune rejected. This extends the applicability of this approach for monitoring T-cell trafficking since it does not depend on the availability of a transgenic T-cell preparation that recognizes the tumor antigen. We have also demonstrated that tumor rejection was correlated with the uptake of labeled T cells, since the infiltration of labeled T cells was only observed in those tumors that went on to regress. In the study of Kircher et al. (13), all ovalbumin-expressing tumors showed stasis or volume reduction and all showed uptake of labeled T cells. Kircher et al. (13) noted in previous studies in which T-cell infiltration of tumors had been assessed histologically that the T cells were observed largely in the tumor periphery. This had been observed in rat mammary tumors and in sections from B-cell non-Hodgkins lymphoma patients, whereas in their melanoma tumor model they observed infiltration throughout the tumor mass. We have confirmed this observation here but in a different tumor model, a mouse lymphoma. The heterogeneous pattern of T-cell recruitment that we observed between 24 and 144 h after cell injection was similar to that observed by Kircher et al. (13). Their observation of a more extensive image hypointensity following cell injection may be explained by their use of a different tumor model or by their use of the OT-1 CD8+ T-cell preparation that is targeted specifically at ovalbumin.

Recently MRI has been used to track in vivo the migration of labeled human natural killer (NK) cells into NIH 3T3 mammary tumors that had been implanted in the mammary fat pad of mice. The tumors expressed the HER2/neu receptor and the NK cells had been engineered to express a chimeric antigen receptor that was specific to HER2/neu (30). The cells were labeled with up to 2.9 pg iron/cell using a cell transfection agent and were readily visible in HER2/neu expressing tumors in vivo 24 h after iv injection of 5×10^6 labeled cells.

In conclusion, we have demonstrated that T cells isolated from immunized animals can be readily labeled with an iron oxide preparation that is simple to prepare and that allows the real time tracking of these cells in vivo using MRI. Tumor infiltration of these labeled T cells was only observed if the tumor was undergoing regression and the cells had been isolated from an animal that itself had rejected its E.G7-OVA tumor. This technique should permit a better understanding of those factors that are important in mediating immune rejection of tumors.

ACKNOWLEDGMENTS

MIK thanks the Ella and Georg Ehrnrooth Foundation, the Emil Aaltonen Foundation, the Finnish Cultural Foundation of Northern Savo, and University of Kuopio for additional financial support.

REFERENCES

1. Yee C, Riddell S, Greenberg P. In vivo tracking of tumor-specific T cells Curr Opin Immunol 2001;13:141–146.
2. Moore MW, Carbone FR, Bevan MJ. Introduction of soluble protein into the class I pathway of antigen processing and presentation. Cell 1988; 54:777–785.
3. Rotzschke O, Falk K, Stevanovic S, Jung G, Walden P, Rammensee H. Exact prediction of a natural T cell epitope. Eur J Immunol 1991;21: 2891–2894.
4. Vasovic LV, Dyall R, Clynes RA, Ravetch JV, Nikolic-Zugic J. Synergy between an antibody and CD8(+) cells in eliminating an established tumor. Eur J Immunol 1997;27:374–382.
5. Dyall R, Vasovic LV, Clynes RA, Nikolic-Zugic J. Cellular requirements for the monoclonal antibody-mediated eradication of an established solid tumour. Eur J Immunol 1999;29:30–37.
6. Shrikant P, Mescher MF. Control of syngeneic tumor growth by activation of CD8+ T cells: efficacy is limited by migration away from the site and induction of nonresponsiveness. J Immunol 1999;162:2858–2866.
7. Helmich B, Dutton R. The role of adoptively transferred CD8 T cells and host cells in the control of the growth of the EG7 thymoma: factors that determine the relative effectiveness and homing properties of Tc1 and Tc2 effectors. J Immunol 2001;166:6500–6508.
8. Gao F, Khammanivong V, Liu W, Leggatt G, Frazer I, Fernando G. Antigen-specific CD4+ T-cell help is required to activate a memory CD8+ T cell to a fully functional tumor killer cell. Cancer Res 2002; 62:6438–6441.
9. Hu, D-E, Beauregard DA, Bearchell MC, Thomsen LL, Brindle KM. Early detection of tumour immune-rejection using magnetic resonance imaging. Br J Cancer 2003;88:1135–1142.
10. Hu, D-E, Dyke SOM, Moore AM, Thomsen LL, Brindle KM. Tumour cell-derived nitric oxide is involved in the immune-rejection of an immunogenic murine lymphoma. Cancer Res 2004;64:152–161.
11. Hu D, Moore A, Thomsen L, Brindle K. Uric acid promotes tumor immune rejection. Cancer Res 2004;64:5059–5062.

12. Lewin M, Carlesso N, Tung, C-H, Tang, X-W, Cory D, Scadden DT, Weissleder R. Tat peptide-derivatized magnetic nanoparticles allow in vivo tracking and recovery of progenitor cells. Nature Biotech 2000;18: 410–414.
13. Kircher, MF, Allport, JR, Graves, EE, Love, V, Josephson, L, Lichtman, AH, Weissleder, R. *In vivo* high resolution three-dimensional imaging of antigen-specific cytotoxic T-lymphocyte trafficking to tumors. Cancer Res 2003;63:6838–6846.
14. Arbab A, Yocum G, Kalish H, Jordan E, Anderson S, Khakoo A, Read E, Frank J. Efficient magnetic cell labeling with protamine sulfate complexed to ferumoxides for cellular MRI. Blood 2004;104:1217–1223.
15. Smirnov P, Gazeau F, Lewin M, Bacri J, Siauve N, Vayssettes C, Cuenod C, Clementi O. In vivo cellular imaging of magnetically labeled hybridomas in the spleen with a 1.5-T clinical MRI system. Magn Reson Med 2004;52:73–79.
16. Fu L, Dravid V, Johnson D. Self-assembled (SA) bilayer molecular coating on magnetic nanoparticles. Appl Surface Sci 2001;181:173–178.
17. Tartaj P, Morales M, Veintemillas-Verdaguer S, Gonzalez-Carreno T, Serna C. The preparation of magnetic nanoparticles for applications in biomedicine. J Phys D Appl Phys 36:R182–R197, 2003.
18. Bont W, De Vries J, Geel M, Van Dongen A, Loos H. Separation of human lymphocytes and monocytes by velocity sedimentation at unit gravity. J Immunol Methods 1979;29:1–16.
19. Funovics M, Kapeller B, Hoeller C, Su H, Kunstfeld R, Puig S, Macfelda K. MR imaging of the her2/neu and 9.2.27 tumor antigens using immunospecific contrast agents. Magn Reson Imaging 2004;22:843–850.
20. Gupta A, Gupta M. Cytotoxicity suppression and cellular uptake enhancement of surface modified magnetic nanoparticles. Biomaterials 2005;26:1565–1573.
21. Frank J, Miller B, Arbab A, Zywicke H, Jordan E, Lewis B, Bryant L, Bulte J. Clinically applicable labeling of mammalian and stems cells by combining superparamagnetic iron oxides and transfection agents. Radiology 2003;223:480–487.
22. Bulte J, Kraitchman D. Monitoring cell therapy using iron oxide MR contrast agents. Curr Pharm Biotech 2004;5:567–584.
23. Hanson H, Donermeyer D, Ikeda H, White J, Shankaran V, Old L, Shiku H, Schreiber R, Allen P. Eradication of established tumors by CD8+ T cell adoptive immunotherapy. Immunity 2002;13:265–276.
24. Chapman A, Rickinson A, Thomas W, Jarrett R, Crocker J, Lee S. Epstein-Barr virus-specific cytotoxic T lymphocyte responses in the blood and tumor site of Hodgkin's disease patients: Implications for a T-cell-based therapy. Cancer Res 2001;61:6219–6226.
25. Yee C, Thompson J, Byrd D, Riddell S, Roche P, Celis E, Greenberg P. Adoptive T cell therapy using antigen-specific CD8+ T cell clones for the treatment of patients with metastatic melanoma: *in vivo* persistence, migration and antitumor effect of transferred T cells. Proc Natl Acad Sci USA 2002;99:16168–16173.
26. Kaech S, Wherry E, Ahmed R. Effector and memory T-cell differentiation: Implications for vaccine development. Nat Rev Immunol 2002;2:251–262.
27. Parish C. Fluorescent dyes for lymphocyte migration and proliferation studies. Immunol Cell Biol 1999;77:499–508.
28. Massoud T, Gambhir S. Molecular imaging in living subjects: Seeing fundamental biological processes in a new light. Genes Dev 2003;17: 545–580.
29. Herschman H. Micro-PET imaging and small animal models of disease. Curr Opin Immunol 2003;15:378–384.
30. Daldrup-Link H, Meier R, Rudelius M, Piontek G, Piert M, Metz S, Settles M, Uherek C, Wels W, Schlegel J, Rummeny E. In vivo tracking of genetically engineered, anti-HER2/neu directed natural killer cells to HER2/neu positive mammary tumors with magnetic resonance imaging. Eur Radiol 2005;15:4–13.